The Effects of WPS on Cleavage Fracture of Ferritic Steels

S. Hadidi-Moud[1] , D.J. Smith[2] and H. Fowler[3]
Department of Mechanical Engineering, University of Bristol, BS8 1TR, UK
Saeid.Hadidi-Moud@Bristol.ac.uk

Abstract

An extensive experimental programme has been carried out to characterise the mechanical parameters and the fracture response of two steels, BS1501 and A533B. These are widely used in pressure vessel technology. The role of load history on improvements in cleavage fracture toughness has been investigated. Finite element analyses have been performed to simulate and verify the findings of the experimental programme. Scatter within experimental cleavage toughness data has been described by using the model proposed by Wallin [1] and combined with Chell [2] model for WPS effect. A stress matching approach to predicting the fracture response of the as received, as well as the warm pre-stressed specimens is also suggested. Using the stress distributions from the finite element analyses prediction of fracture after WPS is examined and results are compared to both the experimental data and those obtained by the combined Chell -Wallin [3] model of failure probability. The significance of residual stress field in enhancing of cleavage fracture toughness following warm pre-stressing has been highlighted.

Keywords: ferritic pressure vessel steels; WPS; finite element; cleavage fracture; residual stress; scatter

1. Introduction

Many engineering components are subjected to "proof" loading prior to service operation. This "proof" loading is often used to demonstrate the integrity of a finished product. One feature of proof loading that has gained recognition is the benefit that may be obtained in improving in-service component reliability particularly when the component is operated at a temperature lower than the proof load. This type of "proof" loading and subsequent low temperature operation is often called warm pre-stressing (WPS). This feature is important when considering a component containing postulated defects. The effect of WPS at an upper shelf temperature on cleavage fracture at a subsequent lower shelf temperature has been studied extensively. A brief review of these studies is given later. There are many different temperature-loading paths to be considered for the component. In laboratory based experimental work three main pre-stressing, cooling and unloading cycles have been studied named as LCF, LCUF and LUCF, where L is pre-load, U is unload, C is cool and F is reload to fracture. Smith and Garwood [4,5] summarised a wide range of experimental results from earlier studies for these different cycles. The LCF cycle provides the largest improvement in toughness with the minimum benefit from warm pre-stressing occurring for the LUCF cycle [6]. As shown schematically in Figure 1, if the load-unload-cool-fracture (LUCF) cycle is applied to a pre-cracked specimen the lower shelf cleavage toughness is increased following WPS on the upper shelf. However the interaction between the WPS and the subsequent toughness distribution has received less attention. This paper presents and summarises the results of detailed investigation into the brittle fracture response of two pressure vessel steels, A533B class 1 and BS1501, following WPS. A series of tests were carried out to determine the scatter in cleavage fracture toughness of these steels. The results were compared with an analytical model developed by Chell and co-workers [2,7,8]. Notably we introduced the Chell model into a simple probabilistic analysis to demonstrate how warm pre-stressing changed failure probability. Without recourse to a probabilistic analysis there arises uncertainty in the interpretation of the results. The experimental programme used single edge notched bend, SEN(B), and compact tension, C(T), specimens. Surprisingly, while the basic analytical models were

[1] Research Associate, Structural Integrity Research Group, University of Bristol, UK / Dr.
[2] Head of Structural Integrity Research Group, University of Bristol, UK / Prof.
[3] Frazer Nash Consultants Company, UK / Dr.

developed over twenty years ago there have been no supporting numerical studies to verify or otherwise these theories. Nonetheless finite element (FE) work has been carried out to examine, for example, the application of the "local approach" to warm pre-stressing [9]. Recent numerical studies considered scatter in fracture toughness using probabilistic models.

To place the work in context, earlier studies on the effects of WPS and probabilistic studies on cleavage fracture toughness are reviewed briefly.

1.1. Overview of WPS effect on cleavage fracture

The warm pre-stress effect theories proposed by Chell [2, 7], based on J-integral, and by Curry [10] based on the Ritchie, Knott, Rice (RKR) model are the main theories used in WPS experimental studies. Using the Chell model, Chell and Haigh [8] proposed a simple lower bound WPS failure criterion. Smith and Garwood [4,11] provided a more detailed review of the effects of WPS on cleavage fracture in pressure vessel steels and also presented results from a comprehensive experimental programme using A533B steel SEN(B) specimens. Results were compared to the theories of Chell [2] and Curry [10], and good overall agreement was found. Reed and Knott [12-14] examined different pre-loading regimes for A533B weld steel using four-point bend specimens. Their findings suggest that the main effect of WPS is associated with a residual stress field at the crack tip. Further investigations include those by Pokrovsky et al [15], Okamura et al [16, 17] and Timofeev and Smirnov [18], Cheng and Noble [19] and Stokle et al [20].

1.2. Overview of probabilistic studies of cleavage fracture

Quantification of the scatter in fracture toughness is generally associated with the use of statistical approaches. These are mostly based on the weakest link theory proposed by Weibull [21,22]. For cleavage fracture the statistical local approach proposed by Beremin [23, 24] forms the basis for the majority of the research work carried out. Other research regarding statistical modelling of cleavage fracture include Wallin [1,25-27], Slatcher [28], Neville [29], Anderson and Stienstra [30], Smith and Garwood [4,11], Landes [31], Holzmann et al [32], Fowler et al [33], Shehu and Nilson [34], Yahya et al [35], Margolin et al [36, 37], O'Dowd et al [38], and Zhang and Knott [39]. They investigated the influence of a range of parameters on scatter in brittle fracture.

1.3. Overview of scatter in toughness following WPS

The only systematic experimental studies to investigate scatter in toughness following WPS is reported by Smith and Garwood [11], and Fowler et al [33]. However, a thorough analysis was not provided to describe the scatter.

Recently Chen et al [40] argued that a primary parameter in enhancement of apparent toughness following WPS is reduction in normal tensile stress due to decrease of the stress triaxiality and strain developing in front of the blunted tip. It was also argued that residual compressive stresses play a secondary role. Their study of the mechanism of WPS effects on toughness includes FE analyses of various WPS cycles to determine the normal stress, plastic strain and stress triaxiality distributions around the crack tip modelled with slight blunting.

In recent numerical studies scatter has been considered using probabilistic models. For example, Stockl et al [20] and Kordish et al [41] incorporated modified probabilistic models developed by Beremin group [23, 24] to predict cleavage fracture following WPS. Stockl et al [20] also compared simulations with experimental results. Their results, linked to finite element analyses, were used to suggest that crack tip blunting is the main feature that provides the improved cleavage toughness following WPS. This argument is inconsistent with the findings from Reed and Knott [13, 14] and Smith and Garwood [11]. Valeta et al [42], Yagawa et al [43] and Lidbury et al [44], among others have also investigated some aspects of WPS effect. In summary, there is a considerable body of work that identifies the essential features of the effects of warm pre-stressing on subsequent fracture response of ferritic steels.

This paper brings together a substantial quantity of recent experimental evidence. Results are compared and assessed using predictions from an analytical model of WPS combined with a statistical model of cleavage fracture proposed by Wallin [1], as well as results obtained from elastic-plastic finite element analyses in conjunction with a stress matching technique that is described later. First, a summary of an experimental programme is briefly explained and the relevant analytical models are summarised and used to assess the experimental results. Second, the FE studies are described and predictions of near crack tip residual stresses are provided. This is followed by the description of a method for determining the effects of warm pre-stressing from the FE analyses. The method is then applied to a stationary crack and to an extended crack and results are assessed in light of the experimental results and analytical procedures.

2. Experiments

2.1. Overview of experimental work

Smith and Garwood [11], and Fowler [3] performed extensive experimental programmes using C(T) and SEN(B) specimens manufactured from parent plates of A533B and BS1501 steels to investigate the WPS effect.

Tests for A533B steel were carried out using 25mm thick compact tension, C(T), and 50mm thick single edge notch bend, SEN(B) specimens. All the SEN(B) specimens were fatigue pre-cracked. The A533B steel SEN(B) specimens were fractured at –170°C. The pre-loading occurred at or close to the estimated limit load, P_L, for the specimen. Initial loading was carried at room temperature and followed by cooling to and fracturing at the low temperature.

A similar test programme was conducted for the BS1501 steel. C(T)25 and SEN(B)50 specimens were fracture tested at –120°C, in the as-received (AR) condition. SEN(B)50 tests at -120°C were fatigue- pre-cracked. Similar to the A533B steel specimens, BS1501 steel C(T) and SEN(B) specimens were pre-loaded at room temperature to about the estimated collapse load.

2.2. Experimental Results

In all tests the stress intensity factor at failure, K_f and at pre-loading, K_I, was determined using the measured maximum load and average crack length after pre-fatigue cracking (according to BS 7448, 1991).

The as-received toughness for the two steels is shown in Figures 2 and 3 as a function of specimen type and temperature. For A533B steel tested at -170°C, Figure 2, the limited tests for C(T)25 lie within the scatter for the larger SEN(B)50 results. Notably, the toughness of the EDM notched C(T)25 specimens was generally higher than the toughness of the pre-fatigue cracked specimens. Similar trends in toughness are shown in Figure 3 for BS1501 steel. The results shown in Figure 2 and 3 act as reference points for the remaining results that explore the influence of prior loading history, specimen type and experimental scatter.

The change in fracture toughness of A533B steel following proof load, is shown in Figure 4 for fracture at –170°C. Results are expressed in terms of the fracture toughness as a function of the pre-load K_1. For a given specimen type there was a general increase in lower shelf toughness following WPS. This was regardless of the geometry or the technique used in pre-cracking of the specimens.

Similar effects were also found for BS1501 steel. The results are shown in Figure 5, for tests at -120°C. The increase in toughness for the C(T) specimens was more notable than for the SEN(B) specimens for this steel.

3. Analytical Models

Two models developed by Chell [2] and Curry [10] remain the main methods for predicting the effects of warm pre-stressing. A detailed review of the models is given by Smith and Garwood [4]. In each model it is essential to determine the relative sizes of the crack tip plastic zones following each loading step. For example, if the plastic zone at the low temperature fracture load is larger than the plastic zones created by pre-loading and unloading the models predict that there is no benefit obtained from warm pre-stressing. Conversely if the fracture plastic zone is within the former plastic zones the near crack tip stresses, strains and displacements are a function of the prior load history. The two models use different underlying assumptions. Curry's model, extended by Smith and Garwood [4,11,45], uses stress superposition. Chell used discrete yielding and displacement superposition to determine the effects of load and temperature history. Details of Chell model, a Displacement superposition model, can be found in Chell and co-workers [2,7,8]. This criterion is used, together with a model for strip yielding [46], to determine the conditions for onset of failure for different loading paths. Chell demonstrated that for LUCF conditions the failure stress intensity factor, K_f, is obtained from:

$$\frac{K_{Ic}^2}{\sigma_{Y2}} = \frac{K_{Ic}^2}{\sigma_{Y1}}\left\{1 - f\left(\frac{R_3}{R_1}\right)\right\} - \frac{K_1^2}{2\sigma_{Y1}}\left\{1 - f\left(\frac{R_3}{R_2}\right)\right\} + \frac{K_f^2}{(\sigma_{Y1} + \sigma_{Y2})} \quad (1)$$

where σ_{Y1} and σ_{Y2} are the yield stresses at the proof load and fracture load temperatures respectively.

Curry [10] proposed an alternative method, a Stress superposition model, for predicting the effect of warm pre-stressing on lower shelf cleavage fracture. Curry's model uses the Ritchie, Knott and Rice (RKR) fracture criterion [47]. The critical stress intensity factor, K_{Ic}, is proportional to the product $\sigma_c \sqrt{r_c}$, where σ_c is a characteristic stress and r_c is a characteristic distance ahead of the crack tip. For the LUCF case with a final fracture plastic zone smaller than prior load and unload plastic zones, the stress distribution at fracture is given by the superposition of the pre-load, unload and reload stages as follows:

$$\sigma_{yy}[K_f] = \sigma_{yy}[K_1, \sigma_{Y1}] - \sigma_{yy}[K_1, 2\sigma_{Y1}] + \sigma_{yy}[K_1, (\sigma_{Y1} + \sigma_{Y2})] \quad (2)$$

where σ_{yy} is the stress component normal to the crack plane. For each loading condition this stress is a function of the current stress intensity factor and the yield stress. Curry [10] suggested using finite element stress distributions from one load case to infer the stress σ_{yy} for the other load cases. Smith and Garwood [4,45] sought an analytical solution using the Hutchinson, Rice and Rosengren (HRR) stress field [48,49] for a power law hardening material. Using equation (2) as a starting point the ratio of the fracture toughness after WPS, K_f, to the as-received toughness, K_{Ic}, is given by:

$$\frac{K_f}{K_{Ic}} = \left(\frac{\sigma_{Y1}}{\sigma_{Y2}}\right)^{m/q}\left\{1 - \left(\frac{\sigma_{Y1}}{\sigma_{Y2}}\right)^{m}\left(\frac{K_1}{K_{Ic}}\right)^{q}\left(1 - 2^m\right)\right\}^{1/q} \quad (3)$$

where $m=(n-1)/(n+1)$ and $q=2(n+1)$ with n the power law hardening exponent.

Unlike the Chell and Curry models, that are based on the local crack tip stress/strain distributions, Smith and Garwood [4] also proposed using a "reference stress" in the net section (or un-cracked ligament) of the component. This provides an approximate description of the global behaviour that leads to differences between pre-stressed and non pre-stressed components. The reference stress approach simply modifies the analytical solution (equation 10) obtained by Smith and Garwood [4] for the model proposed by Curry [10], by replacing the toughness ratio by the reference stress ratio as:

$$\frac{\sigma_{Rf}}{\sigma_{Rc}} = \left(\frac{\sigma_{Y1}}{\sigma_{Y2}}\right)^{m/q}\left\{1 - \left(\frac{\sigma_{Y1}}{\sigma_{Y2}}\right)^{m}\left(\frac{\sigma_{R}}{\sigma_{Rc}}\right)^{q}\left(1 - 2^m\right)\right\}^{1/q} \quad (4)$$

Here the proof load reference stress, σ_R, and the reference stress at fracture, σ_{Rf}, are by definition limited to the yield stresses at the pre-load and the fracture temperatures respectively.

Since the Chell, Curry and Smith-Garwood models can be expressed in terms of the ratios of stress intensity factors, K_f/K_{Ic} and K_1/K_{Ic}, predictions are shown in Figure 6. To determine the curves shown in Figure 6 it was assumed that σ_{Y1} is 530 MPa and σ_{Y2} is 818 MPa for A533B steel at 20°C and –170°C respectively. Also shown are the experimental results from two earlier studies by Reed and Knott [12-14] and Loss et al [50]. Note that in each of these experimental studies the average K_{Ic} at the fracture temperature quoted by each researcher is used to determine the ratios K_f/K_{Ic} and K_1/K_{Ic}.

Overall at low pre-load levels the agreement between the experiments and mode I predictions is good. However at high pre-load levels the models tend to underestimate the WPS effect from the LUCF loading cycle. Later in the paper we will focus on comparing the combined Wallin-

Chell model predictions with stress matching approach based on FE simulations.

4. Analyses

4.1. Comparison with WPS Theories

The wide range of experimental results is first examined using the models developed by Chell [2, 7], Curry [10] and Smith and Garwood [5,45]. All models predict the new toughness, K_f following a proof load or warm pre-stress cycle as:

$$K_f = g\left(K_{Ic}, K_1, \sigma_{Y1}, \sigma_{Y2}\right) \tag{5}$$

Examples of the predictions using the Chell model are shown in Figure 4 for A533B steel at -170°C and in Figure 5 for BS1501 steel at -120°C. For A533B steel values of σ_{Y1} and σ_{Y2} were 530MPa (at 20°C) and 818MPa (at -170°C). Yield strength for BS1501 steel was 358MPa (at 20°C) and 565MPa (at -120°C).

4.2. Statistical Analysis

The number and range of experimental results generated by the test programmes for the two steels provide a database for undertaking a statistical analysis of the results. First an equation developed by Wallin [1] is used to obtain fitted parameters to the as-received experimental results. Second the model is extended to take account of the influence of WPS on lower shelf fracture toughness.

Wallin proposed that the probability of failure, P_f, is given by:

$$P_f\left[K_{Ic}\right] = 1 - \exp\left(-\frac{B}{B_o}\left\{\frac{K_{Ic} - K_{\min}}{K_o - K_{\min}}\right\}^n\right) \tag{6}$$

where B_0 and K_0 are normalisation constants. B_0 can be any desired reference thickness and K_0 corresponds to a 63.2 percent fracture probability for thickness B_0. Wallin [1] also introduced a lower limiting value, K_{min}, below which cleavage fracture is considered impossible.

Equation (6) was fitted to the as-received experimental results for A533B steel at -170°C as shown in Figure 7, and for BS1501 steel at -120°C shown in Figure 8. It was assumed that K_{min} and K_0 were free variables. The exponent n in equation (6) is 4 and the reference thickness B_0 is 50mm. The calibrated parameters K_{min} and K_0 are given as 6.0 and 64.0 for A533B at –170°C and 5.0 and 70.0 for BS1501 steel at –120°C, respectively.

4.3. Using WPS with a Statistical Analysis

To account for scatter in the WPS effect, the Chell model is used to predict changes in K_{min} and K_0 following a pre-stressing event of average magnitude. For example, the average pre-load stress intensity factor, K_1, for A533B at -170°C using SEN(B)50 specimens as shown in Figure 4 was 89MPa√m. Similarly, following WPS the fitted parameters to the as-received data, K_{min} and K_0, are modified using equation (5) (and replacing K_{Ic} with either K_{min} or K_0) so that:

$$K_{\min,f} = g\left(K_{\min}, K_1, \sigma_{Y1}, \sigma_{Y2}\right) \tag{7}$$

and

$$K_{o,f} = g\left(K_o, K_1, \sigma_{Y1}, \sigma_{Y2}\right) \tag{8}$$

The probability of failure after WPS is now given by

$$P_f\left[K_f\right] = 1 - exp\left(-\frac{B}{B_o}\left\{\frac{K_{Ic} - K_{min,f}}{K_{o,f} - K_{min,f}}\right\}^n\right) \tag{9}$$

Predicted failure probabilities using equation (9) combined with equations (7) and (8) are shown for A533B steel at -170°C in Figure 7 and for BS1501 steel at -120°C in Figure 8. Values quoted earlier for the yield strengths of the two materials were used in equations (7) and (8). For A533Bsteel the predicted failure probability is overestimated or conservative compared to the experimental results using SEN(B)50 specimens. Failure probability for BS1501 steel experimental results for SEN(B)50 and C(T)25 specimens was also examined. Predictions are shown in Figure 8, one based on the reference thickness, B_0=50mm and the second for B=25mm. Although there were only limited experimental results using SEN(B)50 specimens the predictions at the reference thickness B_0=50mm are in good agreement with these experiments. The prediction for B=25mm was made by scaling the failure probability for B_0=50mm using equation (9). The predicted failure probability is higher than obtained in the experiments.

5. Finite Element Studies

The results of numerical simulations of the effects of warm pre-stress load histories on the candidate steels are presented in this section. The ABAQUS-CAE (version 6.2) [51] finite element code was used throughout the study. Elastic-plastic finite element studies were performed to provide an insight into the crack tip stress fields during the warm pre-stress cycle and at fracture. The FE models analysed include two-dimensional models of SEN(B) and C(T) with appropriate mesh refinement at the crack tip area to obtain consistent results. Plane strain analyses were carried out using both isotropic and kinematic hardening laws with the ratio of crack length to the crack width, a/W, equal to 0.5. The results from the FE simulations are first presented in terms of the residual stresses generated after unloading following pre-loading. A method of predicting fracture following warm pre-stress in the FE simulations is then presented.

5.1 Residual Stresses

The first step in the FE analysis was to examine the residual stresses developed after pre-loading and unloading. The results, shown in Figure 9 indicate that the residual stress generated after unloading, especially the peak near tip residual stress, is strongly dependent on the material model and stress state. Although not shown in Figure 9, when residual stress fields from different pre-loads are compared, the peak residual stress is the same and the region of compressive residual stress increases with increasing pre-load.

5.2 Prediction of Fracture after WPS

Finite element simulations for these experiments were carried out for both steels (BS1501 at –120°C and A533B at –170°C) . The results were broadly similar for a variety

of loading conditions. As with the residual stress predictions, simulations were carried out for both the SEN(B) and C(T) geometry. Finite element simulations of fracture were performed for two experimental load histories, the as-received (AR) and LUCF conditions. The analyses simulating the LUCF cycle were performed in three discrete steps. Initially the specimen was loaded to the maximum experimental applied load at room temperature. It was then incrementally unloaded to zero load at the same temperature. Finally the specimen was cooled down to the fracture temperature and reloaded to fracture. The analyses were performed using both the isotropic and kinematic hardening laws.

A typical HRR maximum principal stress distribution corresponding to a fracture load in the as-received state and determined from Ramberg-Osgood power law relationship, is shown in Figure 10. The *J* integral was determined directly from the ABAQUS FE analysis. Also shown is the stress distribution corresponding to the as-received fracture condition obtained from the FE analysis. Both the HRR and FE stress distributions correspond to a sharp tip crack and small displacements. For $r/(W-a)<0.002$ there is excellent agreement between the HRR and FE stress distributions.

In the LUCF cycle, on reloading at the lower temperature after unloading, it was found that the differences in the maximum principal stress distribution for kinematic and isotropic hardening became small and the stress distributions essentially the same at sufficiently higher loads. The stress distributions for the two hardening models for an intermediate loading at $K=40.6$ MPa$\sqrt{m}$, and at the fracture load with $K_f=66$ MPa$\sqrt{m}$ are shown in Figure 10. In each load case the differences between the hardening models are small.

At different levels of reloading between $K=40.6$ MPa$\sqrt{m}$ and $K_f=66$ MPa$\sqrt{m}$ the FE results were assessed to determine the applicability of the RKR model to the LUCF cycle. It was found that the reloading and as-received stress distributions could be matched for distances $r/(W-a)<0.002$ for a range of stress intensity factors between *50* and *66* MPa$\sqrt{m}$. In contrast, the stress distribution after WPS, that matched the as-received case, for distances as far as possible ahead of the crack tip, corresponded to a fracture load that was close to the experimental conditions. The matched stress distributions for kinematic and an isotropic hardening conditions are shown in Figure 10. These results suggest that predictions of the WPS effects can be made using the stress superposition models at a limited distance ahead of the crack tip. However the results are ambiguous since there are many solutions between $K=50$ and *60* MPa$\sqrt{m}$. Alternatively, when complete stress matching is made between the as-received and WPS maximum principal stresses, the resulting fracture load following WPS is well defined. Based on the simulated stress fields for the as-received and warm pre-stressed conditions it was possible for the cleavage fracture toughness of a component to be predicted by matching the stress field formed on reloading to the stress field corresponding to the material's critical stress intensity factor. Many finite element analyses were then performed to examine this further by first simulating pre-loading events of different magnitudes at room temperature, unloading to zero load and reloading incrementally at low temperature. At each reload increment, the crack tip stress field was compared to the stress field corresponding to the as-received cleavage fracture toughness. Predictions of the critical stress intensity factor at maximum load were made using the load achieved at the increment where the stress distributions were in best agreement with the stress field for the as-received toughness.

The results of these FE predictions are summarised in Figure 11, where the reloading maximum load fracture toughness determined by stress matching with as-received stress fields is shown as a function of the proof load K_I. The results correspond to the fracture behaviour of A533B steel at –170°C. Also shown are predictions using the Curry [10] and Chell [2,7,8] models described earlier. For clarity the results of the Curry model are shown only for an as-received toughness of *47.4* MPa$\sqrt{m}$ and similar trends occur between the Chell and Curry models for higher levels of as-received toughness. Overall the FE analysis and the Chell model predict a larger increase in toughness than the Curry model for all levels of pre-load. This is similar to the results shown in Figure 6. The FE predictions based on stress matching generally agree with the Chell model predictions at low levels of pre-load. At higher pre-loads in the LUCF cycle the FE analysis provides a larger increase in maximum load toughness compared with the analytical models.

6. Discussion

Under fracture conditions the critical stress intensity factor for both steels improved by pre-loading at room temperature prior to fracture at low temperatures.

Based on mean values of toughness the experimental evidence suggests for A553B steel there is only a limited influence of thickness on toughness following WPS. For example, results in Figure 10 reveal similar scatter using SEN(B)50 and C(T)25 specimens. In contrast the influence of thickness was more marked for BS1501 steel. This is shown in Figure 8 for tests at -120°C using SEN(B)50 and C(T)25 specimens.

Although there is a wide range of previous studies on the influence and importance of the warm pre-stress effect there is considerable difficulty in assessing the success of various models. This is mainly due to the inherent scatter in cleavage toughness of steel. For instance, Reed and Knott [12] in their WPS studies on A533B weld metal found the correlation between observed and predicted values not to be very good, although general trends could be found. Here in this paper a model has been developed that combines an empirical model [1] for the cleavage fracture toughness together with a model for the effect of WPS [2]. In principle for a given thickness the experimental results support the model predictions. There is also limited evidence that introducing a thickness correction into the model also produces conservative predictions of the probability of failure. However, the statistical model for cleavage fracture toughness following WPS is developed here on the premise that the size and shape of the distribution of cleavage initiators are unchanged.

In relation to analytical models, the main feature in the Chell model [2,7] is that warm pre-stressing provides a

zone of "locked in" dislocations associated with the local residual stresses ahead of the crack tip. The model does not include crack tip blunting. When there is good agreement between the model and experiments as shown for A533B steel at -170°C and BS1501 steel at -120°C the main improvement in toughness following WPS arises from the presence of residual stresses. This supports the findings of Reed and Knott [12-14] that residual stress is the main factor in WPS effects.

Several researchers (e.g. Pokrovsky [15] and Cheng and Noble [19]) suggest the influence of crack tip blunting and local strain hardening. There is no direct evidence that this is the case for these conditions and it can only be inferred that these maybe contributing factors. The results of the finite element analyses have revealed a number of important features about the effects of warm pre-stressing on cleavage fracture. The predicted increase in toughness after WPS are not startlingly different from those developed by a number of theoretical models. However, the FE results have allowed us to examine a number of the underlying assumptions used in the analytical models.

Throughout the FE analysis it was assumed that fracture of the as-received material was associated with the maximum principal stress distribution in the plane normal to the crack and directly ahead of the crack. In the RKR fracture model [47], fracture takes place when a critical stress, σ_c is achieved at a characteristic (or critical) distance, r_c, ahead of the crack tip. In other words a single point on the maximum principal stress distribution is chosen. For the two steels studied here typical distances for r_c are about 150 microns [3]. In Figures 10 and 11 this corresponds to a normalised distance of 0.003. The essential feature of our FE studies is that at this distance an unambiguous matching of the principal stress after WPS could not be obtained by matching to the critical stress for onset of fracture in as-received condition. This was irrespective of the material hardening model used in the FE analysis. These findings suggest that the stress superposition approach developed by Curry [10] and extended by Smith and Garwood [45] is not an appropriate model.

In contrast, when matching of the maximum principal stresses for the as-received and WPS cases is extended for larger distances ahead of the crack tip (and outside of the plastic zone developed in each case), FE predictions of the WPS fracture load (and stress intensity factor) are very similar to the displacement superposition model developed by Chell [2] at low pre-load levels. In Chell's model the J-integral is shrunk onto the yielded region and contains only the elastic displacements when the reloading plastic zone is within the overload plastic zone. The elastic displacements in this region arise from stress field developed outside of the plastic zones.

The stress matching method developed here also suggests that if an analytical method is to be developed, other than the displacement superposition method developed by Chell, then terms other than the singular HRR field are required. For example, it is evident that the pre-loading and unloading introduces a compressive residual stress field ahead of the crack tip that extends ahead of the crack tip to about 2% of the un-cracked ligament (as shown in Figure 10). On reloading at the lower temperature the stress field interacts with these residual stresses. Close to the crack tip the onset of plasticity during re-loading effectively diminishes the presence of the residual stresses. However, further away there is only elastic superposition of the compressive residual and the tensile applied stress. This in turn provides an enhancement and increases the load at fracture after WPS that is greater than the as-received fracture load.

When reloading after WPS the near crack tip residual stresses are redistributed due to plasticity created during reloading. Consequently, the details of the material hardening model close to the crack tip appear to be unimportant even though very different residual stress fields are developed near to the crack tip for each hardening model as shown in Figures 9 and 10. Furthermore, at larger distances from the crack tip the residual stress following WPS arises from elastic recovery alone and is not influenced by the hardening model. For example this can be seen in Figure 10 for normalised distances greater than 0.006.

The results of the FE analysis presented here indicate that the presence of the residual stresses generated by proof loading is the main reason for the enhancement in the toughness compared with the as-received toughness. The excellent agreement between the FE results and the Chell model at low levels of proof loading after proof loading also reinforces the argument that the residual stresses are the main underlying feature of the WPS effect.

The results of the FE analysis, Figure 7, revealed that the predicted toughness after WPS (and noting that the predictions were made assuming stress matching) was greater than predicted by Chell's [2,7,8] displacement superposition model. Furthermore, the residual stresses that contribute to the improvement are not those directly at the crack tip, but those at some distance outside of the dominant HRR field. These results together with the comprehensive experimental results suggest that neither crack tip blunting nor strain hardening plays an important role in the improvement in toughness following warm pre-stress.

7. Concluding Remarks

Warm pre-stressing or prior loading at room temperature, followed by fracture at lower shelf temperatures, leads to improvements in fracture toughness of A533B and BS1501 steels. This is irrespective of thickness.

A combined probability of failure and analytical WPS model provided conservative estimates of the probability of failure following warm pre-stressing.

Enhancement in cleavage fracture toughness following WPS can be predicted by matching the stresses away from the crack tip based on the results obtained from FE analyses for the AR and WPS conditions.

Assuming that cleavage fracture is characterised by the distribution of the maximum principal stress directly ahead of the crack tip, the results from the FE analysis have shown that the contributing factor to the benefit provided by WPS is the residual stress.

Acknowledgements

This work was supported by EPSRC and in collaboration with TWI Ltd, British Energy, the Health and Safety Executive, Rolls-Royce and Power Engineering Plc. We would like to particularly thank Steve Garwood and Keith Bell, both formerly at TWI and Amin Mohammed (still at TWI) for their support and advice during this work. Saeid Hadidi-Moud would like to thank Ferdowsi University of Mashhad, Iran for granting him permission to participate in this work.

References

[1] Wallin K. Statistical Modelling of Fracture in the Ductile-to-Brittle Transition Region. In: Blauel JG, Schwalbe KH, editors, Defect Assessment in Components, Fundamentals and Applications, ESIS / EGF 9, Mechanical Engineering Publications, London, 1991. p. 415-445.

[2] Chell GG, Haigh JR, Vitek V. A theory of warm pre-stressing: experimental validation and the implications for elastic plastic failure criteria. Int. J. Fracture. 1981;17(1):61-81.

[3] Fowler H. PhD Thesis: The influence of warm pre-stressing and proof loading on the cleavage fracture toughness of ferritic steels. University of Bristol. 1998

[4] Smith DJ, Garwood SJ. The Significance of Prior Overload on Fracture Resistance: A Critical Review. Int. J. Press. Ves. & Piping. 1990;41:255–296.

[5] Smith DJ, Garwood SJ. Application of theoretical methods to predict overload effects on fracture toughness of A533B steel. Int. J. Pres. Ves. & Piping. 1990;41:333-357.

[6] Burdekin FM, Lidbury DPG. Views of TAGSI on the current position with regard to benefits of warm pre-stressing. Int. J. Pres. Ves. & Piping. 1999;76:885-890.

[7] Chell GG. Some Fracture Mechanics Applications Of Warm Pre-stressing To Pressure Vessels. In: Proc. 4th Int. Conf. Pres. Ves. Technology. IMechE, 1980. p. 117-124.

[8] Chell GG, Haigh JR. The Effect of Warm Pre-stressing on Proof Tested Pressure Vessels. Int. J. Pres. Ves. & Piping. 1986;23:121–132.

[9] FM Beremin. "A local criterion for cleavage fracture of a nuclear pressure vessel steel," J. Metall. Trans. A. 1983;14A:2277-2287.

[10] Curry DA. A Micro-mechanistic Approach to the Warm Pre-stressing of Ferritic Steels. Int. J. Fracture. 1981;17(3):335-343.

[11] Smith DJ, Garwood SJ. Experimental Study of Effects of Prior Overload on Fracture Toughness of A533B Steel. Int. J. Pres. Ves. & Piping. 1990;41:297-331.

[12] Reed PAS, Knott JF. An Investigation Of The Warm Pre-stressing (WPS) Effect In A533B Weld Metal. Fatigue Fract. Engng. Mater. & Struct. 1992;15(12):,1251-1270.

[13] Reed PAS, Knott JF. Investigation of the Role of Residual Stress in the Warm Pre-stress (WPS) Effect Part I- Experimental, Fatigue Fract. Engng. Mater. Struct. 1996;19(4):485-500.

[14] Reed PAS, Knott JF. Investigation of the Role of Residual Stress in the Warm Pre-stress (WPS) Effect Part II- Analysis, Fatigue Fract. Engng. Matr. Struct. 1996;19(4):501-513.

[15] Pokrovsky VV, et al. The Influence of Plastic Pre-stressing on Brittle Fracture Resistance of Metallic Materials with Cracks. Fatigue Fract. Engng. Mater. Struct. 1995;18,(6):731-746.

[16] Okamura H, et al. Experimental Verification of Warm Pre-stressing Effect under pressurised thermal shock (PTS) Event. J.Pres.Ves. Technology. Transactions of ASME. 1994;116:267-273.

[17] H. Okamura H, et al. Further Experimental Verification of Warm Pre-stressing Effect under pressurised thermal shock (PTS). J. Pres. Ves. Technology. 1996;118:174-180.

[18] Timofeev BT, Smirnov VI. Calculated and experimental estimation of preliminary loading effect at elevated temperatures on fracture toughness of pressure vessel materials, Int J. pres. Ves. & Piping. 1995;63:135-140.

[19] Cheng J, Noble FW. The Warm Pre-stressing Effect in Steels Undergoing Intergranular Fracture, Fatigue Fract. Engng. Matr. Struct. 1997; 20(10):1399-1411.

[20] Stöckl H, Böschen R, Schmitt W, Varfolomeyev I, Chen JH. Quantification of the Warm Pre-stressing Effect in a Shape Welded 10 MnMoNi 5-5 Material, Engineering Fracture Mechanics, 2000;67(2):119-137.

[21] Weibull WA. A statistical theory of the strength of materials. Roy. Swed. Inst. Engng. Res. 1939;151:5-45

[22] Weibull W. A Statistical Distribution Function of Wide Applicability. J. Applied Mechanics. Transactions of ASME. 1951;18:293-296..

[23] FM Beremin. Numerical modelling of warm pre-stress effect using a damage function for cleavage fracture. Procs. 5th int. Conf. Fracture (ICF5). Oxford Pergamon. 1981;2.

[24] FM Beremin. "A local criterion for cleavage fracture of a nuclear pressure vessel steel," J. Metall. Trans. A. 1983;14A:2277-2287.

[25] Wallin K, Saario T, Törrönen K. Statistical Model for Carbide Induced Brittle Fracture in Steel. Metal Science, 1984;18:13-16.

[26] Wallin K. The scatter in K_{Ic} results. Engng. Fracture Mech. 1984;19(6):1085-1093.

[27] Wallin K. The size effect in K_{Ic} results. Engng. Fracture Mech. 1985;22(1):149-163.

[28] Slatcher S. A Probabilistic Model for Lower–Shelf Fracture Toughness –Theory and Application. Fatigue Fract. Engng. Mater. Struct. 1986;9(4):275–289.

[29] Neville DJ. Statistical Analysis of Fracture Toughness Data. Engng. Fracture Mech. 1987;27(2):143–155.

[30] Anderson TL, Stienstra D. A model to Predict the Sources and Magnitude of Scatter in Toughness Data in the Transition Region. J. Testing & Evaluation, JTEVA, 1989;17(1):46-53.

[31] Landes JD. A two criteria statistical model for transition fracture toughness. Fatigue Fract. Engng. Mater. Struct., 1993;16(11):1161-1174.

[32] Holzmann M, Man J, Valka L, Vlach B. R-curves and fracture toughness transition behaviour at static, rapid and impact loading of Cr-Ni-Mo-V reactor pressure vessel steel. Int. J Pres. Ves. & Piping. 1995;62:39-47.

[33] Fowler H, Smith DJ, Bell K. Scatter in Cleavage Fracture Toughness Following Proof Loading. In: advances in fracture research, Proc. 9th Int. Conf. Fracture (ICF 9). 1997;5:2519-2526.

[34] Shehu S, Nilson F. Two parameter description of crack growth initiation including thickness effects through probabilistic modelling. Fatigue Fract. Engng. Mater. Struct., 1997;20(2):179-199.

[35] Yahya OML, Borit F, Piques R, Pineau A. Statistical modelling of inter-granular brittle fracture in a low alloy

steel, Fatigue Fract. Engng. Mater. Struct. 1998;21(12):1485-1502.
[36] Margolin BZ, Gulenko AG, Shvetsova VA. Probabilistic model for fracture toughness prediction for nuclear pressure vessels. Int. J. Pres. Ves. & Piping. 1998;75:307-320.
[37] Margolin BZ, Gulenko AG, Shvetsova VA. Improved probabilistic model for fracture toughness prediction based on the new local fracture criteria. Int J Pres. Ves. & piping. 1998;75:843-855.
[38] O'Dowd NP, Lei Y, Busso EP. Prediction of cleavage failure probabilities using the Weibull stress. Engng. Fracture Mech. 2000;67(2):87-100.
[39] Zhang XZ, Knott JF. The statistical modelling of brittle fracture in homogeneous and heterogeneous steel microstructures. Acta Materialia. 2000;48(9):2135-2146.
[40] Chen JH, Wang VB, Wang GZ, Chen X. Mechanism of effects of warm pre-stressing on apparent toughnes of precracked specimens of HSLA steels. Engng. Fracture Mech. 2001;68(2):1699-1686.
[41] Kordisch H, Boschen R, Blauel JG, Schmitt W, Nagel G. Experimental and Numerical investigations of the Warm pre-stressing (WPS) Effect Considering Different Load paths, Nuclear Engineering & Design, 2000;198:89-96.
[42] Valeta MP, Sainte Catherine C, Barbier G, Lefevre W, Eisele U, Bhandari S. Structurel behaviour during a PTS transient taking into account the WPS effect. Int. J. Pres. Ves. & Piping. 2001;78:137-146.
[43] Yagawa G, Yoshimura S, Soneda N, Hirano M. Probabilistic fracture mechanics analyses of nuclear pressure vessels under PTS events. Nuclear Engineering and Design. 1997;174:91-100.
[44] Lidbury DPG, Bass BR, Bhandari S, Sherry AH. Key features arising from structural analysis of the NESC-1 PTS benchmark experiment. Int. J. Pres. Ves. & Piping. 2001;78:225-236.
[45] Smith DJ, Garwood SJ. The Application of Fracture Mechanics to Assess the Significance of Proof Loading. In: Ernst HA, Saxena A, McDowell L, editors. Fracture Mechanics: 22nd Symposium ASTM STP 1131, Philadelphia. 1992;1:833-849.
[46] Bilby BA, Cotterell AH, Swinden KH. The Spread of Plastic Yield From a Notch. Proc. Royal Soc. A. 1963;272:304 – 314.
[47] Ritchie, R. O., Knott, J. F., and Rice, J. R., On The Relationship Between Critical Tensile Stress and Fracture Toughness in Mild Steel. Journal of
Mechanics and Physics of Solids, 1973; 21:395 – 410.
[48] Hutchinson, J. W., Singular Behaviour at the End of a Tensile Crack in a Hardening Material. Journal of the Mechanics and Physics of Solids, 1968;16:13 – 31.
[49] Rice, J. R., and Rosengren, G. F., Plane Strain Deformation Near A Crack Tip in a Power Law Hardening Material. Journal of Mechanics and Physics of Solids, 1968;16:1 – 12.
[50] Loss FJ, Gray RAJr, Hawthorne JR. Significance of Warm Pre-stress to Crack Initiation During Thermal Shock. Nuclear Engineering and Design. 1978;46:3985 – 408.
[51] Hibbit, Karlsson, Sorensen, Inc., ABAQUS/CAE, Version 6.2, 2001

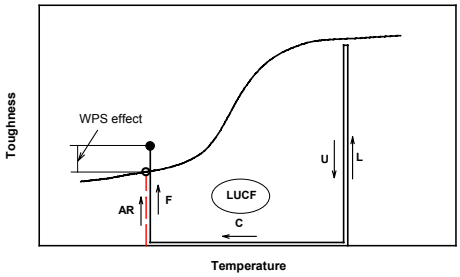

Fig. 1. Schematic LUCF compared to as-received fracture

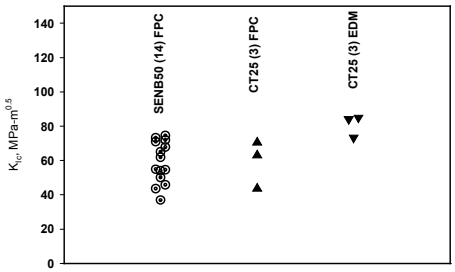

Fig. 2. As-Received fracture toughness of A533B steel, SEN(B) and C(T) specimens at -170°C

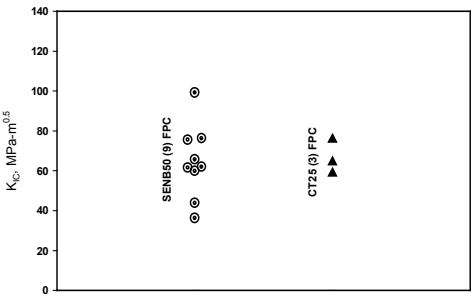

Fig. 3. As-Received fracture toughness of BS1501 steel, SEN(B)50 & C(T)25 specimens at -120°C

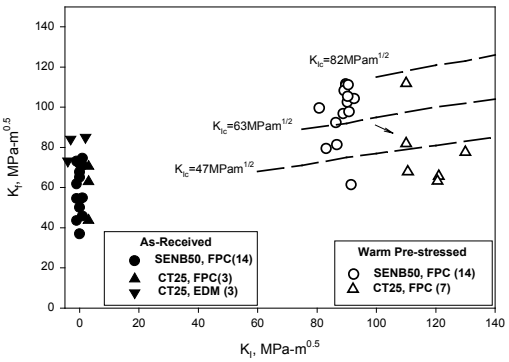

Fig. 4. Fracture toughness of A533B steel at -170°C, before and after LUCF cycle

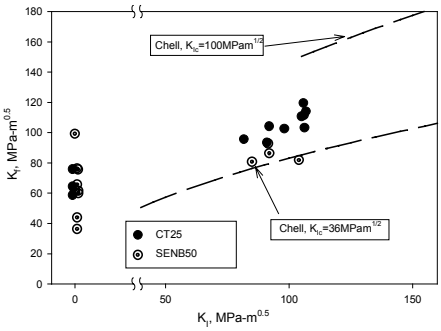

Fig. 5. Fracture toughness of BS1501 steel at -120°C, before and after single LUCF cycle

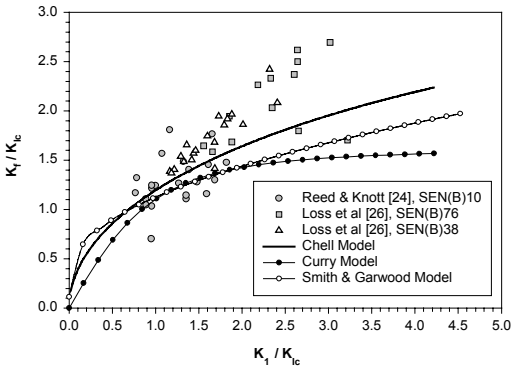

Fig. 6. Comparison between experimental data and theoretical predictions of WPS effect for A533B steel following an overload (K_1) at 20°C

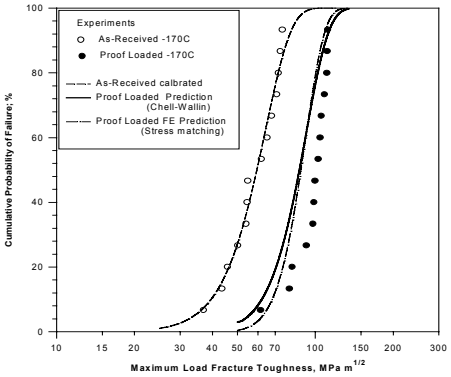

Fig.7. Fracture Toughness of A533B Steel for 50mm Thick SEN(B) Specimens fractured at -170°C

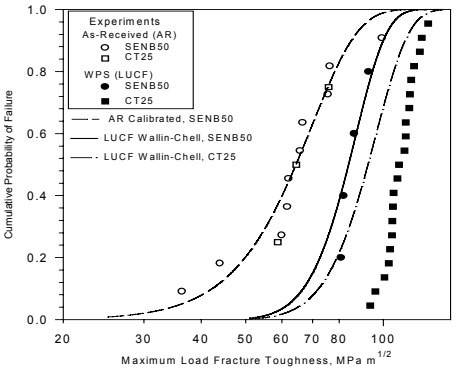

Fig. 8. Fracture Toughness of BS1501 Steel at -120°C

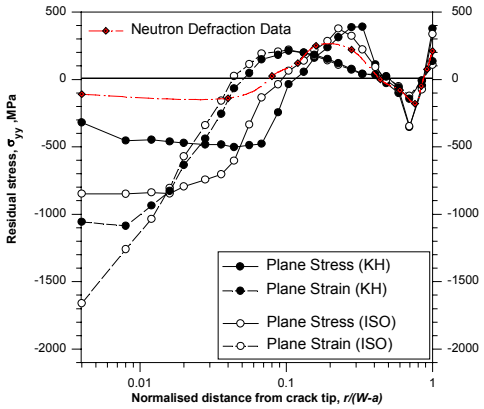

Figure. 9. Distribution of normal to the crack plane residual stresses for plane stress and plane strain conditions for SEN(B) with *a/W=0.5* and *(W-a)*=25 mm KH=Kinematic Hardening, ISO=Isotropic Hardening

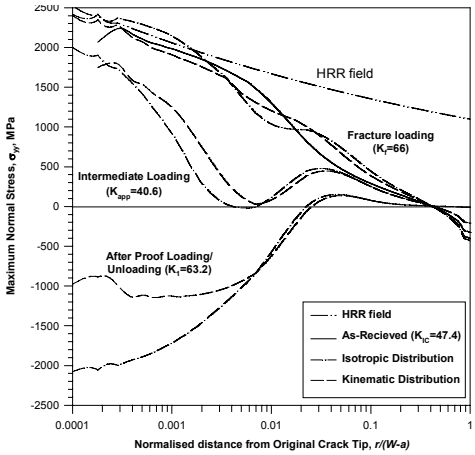

Fig. 10. Comparison of stress distributions in the crack tip region for isotropic and kinematic hardening materials for plane strain conditions for SEN(B) A533B steel at -170°C with *a/W=0.5*, *W=100mm* and *(W-a)=50mm*

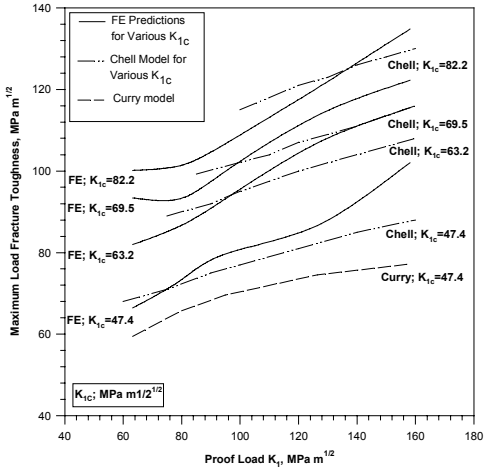

Figure 11. Comparison between the WPS effect predictions from FE analysis and Chell and Curry models for A533B steel for preload at 20°C and fracture at -170°C